blence to the ligand to metal charge-transfer chemistry well established for several classical coordination systems.[35] As stated earlier, X → Re and X → CO CT states often exhibit >1-eV shift to lower energy on replacing the Cl atom by the I atom,[29,31] and, thus, one of these levels may well be reached on excitation of *cis*-IRe(CO)$_4$L at 313 nm. Nonetheless, this photochemical dimerization reaction of the iodide compounds significantly contributes to the disparities observed in the 300–350-nm regions of the absorption and excitation spectra.

Concluding Remarks

Obtained electronic absorption, emission, excitation, and photochemical data fully support $^1A(e^4b_2^2) \rightarrow {}^{1,3}E(e^3b_2^2a_1^1)$ assignments for the lowest lying excited states of *cis*-XRe(CO)$_4$L (X = Cl, I; L = pip, PPh$_3$) complexes. The absence of emission from the $^1A \rightarrow {}^{1,3}E$ LF levels of the parent XRe(CO)$_5$ compounds is thought to be caused by efficient internal quenching processes involving close-lying (X, π)e → π^*(CO) or (X, π)e → $a_1(d_{z^2})$ charge-transfer levels.

This observation of luminescence from the *cis*-XRe(CO)$_4$L derivatives is significant in that these are the first demonstrated examples of radiative decay in fluid solution from the LF states of organometallic complexes. Clearly, the lowest lying LF states of organometallic complexes need not necessarily be dominated by radiationless processes. There are a wide range of transition-metal organometallic complexes known to exhibit lowest lying LF levels, and these results suggest that further studies of their photophysical properties may be informative.

Acknowledgment. We acknowledge the donors of the Petroleum Research Fund, administered by the American Chemical Society, for support of this research.

Registry No. *cis*-ClRe(CO)$_4$(pip), 113975-87-4; ClRe(CO)$_5$, 14099-01-5; *cis*-ClRe(CO)$_4$(PPh$_3$), 15189-56-7; *cis*-IRe(CO)$_4$(pip), 113975-88-5; [IRe(CO)$_4$]$_2$, 15189-53-4; *cis*-IRe(CO)$_4$(PPh$_3$), 15189-55-6; IRe(CO)$_5$, 13821-00-6.

Supplementary Material Available: Table of infrared spectral data in the carbonyl stretching region for XRe(CO)$_5$ and *cis*-XRe(CO)$_4$L complexes (1 page). Ordering information is given on any current masthead page.

(35) (a) Penkett, S. A.; Adamson, A. W. *J. Am. Chem. Soc.* **1965**, *87*, 2514. (b) Caspari, G.; Hughes, R. G.; Endicott, J. F.; Hoffman, M. Z. *J. Am. Chem. Soc.* **1970**, *92*, 6801. (c) Kelly, T. L.; Endicott, J. F. *J. Am. Chem. Soc.* **1972**, *94*, 1797. (d) Natarajan, P.; Endicott, J. F. *J. Am. Chem. Soc.* **1973**, *95*, 2470. (e) Ferraudi, G.; Endicott, J. F. *J. Am. Chem. Soc.* **1973**, *95*, 2371. (f) Endicott, J. F.; Ferraudi, G. J.; Barber, J. R. *J. Am. Chem. Soc.* **1975**, *97*, 219.

Rupture and Repair of the Porphyrin Inner Core: Carbon–Nitrogen Bond Breaking and Formation in Ruthenium Complexes of an N,N′-Bridged Porphyrin

Alan L. Balch,* Yee-Wai Chan, Marilyn M. Olmstead, Mark W. Renner, and Fred E. Wood

Contribution from the Department of Chemistry, University of California, Davis, California 95616. *Received September 8, 1987*

Abstract: Treatment of the *N,N′*-vinyl-bridged porphyrin **1** with $Ru_3(CO)_{12}$ yields three products: the carbene complex TPPRu{C=C(*p*-ClC$_6$H$_4$)$_2$} (**3**) (TPP is the dianion of tetraphenylporphyrin), and two Ru(II) dicarbonyl complexes **4** and **5** in which the N,N′-bridge remains intact, but the ruthenium has inserted into a pyrrole C–N bond. Complexes **4** and **5** differ in that **4** contains the C=C(*p*-ClC$_6$H$_4$)$_2$ N,N′-bridge, while **5** contains a CHCH(*p*-ClC$_6$H$_4$)$_2$ N,N′-bridge. Spectroscopic data (^{1}H NMR, UV/vis, infrared) for the three products are reported. Crystals of **4**, {TPPCHCH(*p*-ClC$_6$H$_4$)$_2$}Ru(CO)$_2$·$^1/_2$CH$_2$Cl$_2$, crystallize in the monoclinic space group $P2_1/c$ with a = 12.633 (7) Å, b = 19.293 (10) Å, c = 19.820 (9) Å, β = 95.59 (3)°, Z = 4 at 130 K. The structure was refined to R = 0.079 for 640 parameters and 4172 reflections. The ruthenium is six-coordinate with two cis carbon monoxide ligands, bonds to two normal pyrrole groups, and bonds to the C and N of the ring-opened pyrrole. The damaged porphyrin is no longer planar. Upon heating, both **4** and **5** undergo C–N bond formation to reform the porphyrin ring.

The stability of the porphyrin macrocycle is one of the causes of its widespread utility in biology. Most chemical attack on porphyrins that alters the nature of the macrocycle involves reactions on the porphyrin periphery.[1,2] Reactions at the interior of the porphyrin are restricted to protonation, metalation,[3] N-akylation or N-arylation,[4] or N-oxidation.[5] These reactions, however, leave the four pyrrole rings intact while adding groups to the pyrrole nitrogen atoms. Here we describe novel reactions which lead to the rupture of the porphyrin inner core through the cleavage of the pyrrole C–N bond by a metal atom (ruthenium). Remarkably, however, this rupture is repairable, and the full porphyrin structure can be restored. A brief account of a portion of this work has appeared.[6]

Scheme I

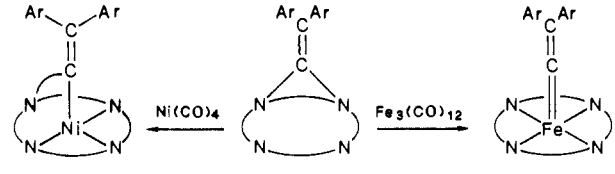

(1) Fuhrhop, J.-H. In *Porphyrins and Metalloporphyrins*; Smith, K. M., Ed.; Elsevier: Amsterdam, 1975; p 625.
(2) Fuhrhop, J.-H. In *The Porphyrins*; Dolphin, D., Ed.; Academic: New York, 1978; Vol. 2, p 131.
(3) Buchler, J. W. In *The Porphyrins*; Dolphin, D., Ed.; Academic: New York, 1978; Vol. 1, p 390.
(4) Jackson, A. H. In *The Porphyrins*; Dolphin, D., Ed.; Academic: New York, 1978; Vol. 1, p 341.
(5) Andrews, L. E.; Bonnett, R.; Ridge, R. J.; Appleman, E. H. *J. Chem. Soc., Perkin Trans. 1* **1983**, 103. Balch, A. L.; Chan, Y. W.; Olmstead, M. M.; Renner, M. W. *J. Am. Chem. Soc.* **1985**, *107*, 6510. Balch, A. L.; Chan, Y. W.; Olmstead, M. M. *J. Am. Chem. Soc.* **1985**, *107*, 6510.
(6) Chan, Y. W.; Wood, F. E.; Renner, M. W.; Hope, H.; Balch, A. L. *J. Am. Chem. Soc.* **1984**, *106*, 3380.

0002-7863/88/1510-3897$01.50/0

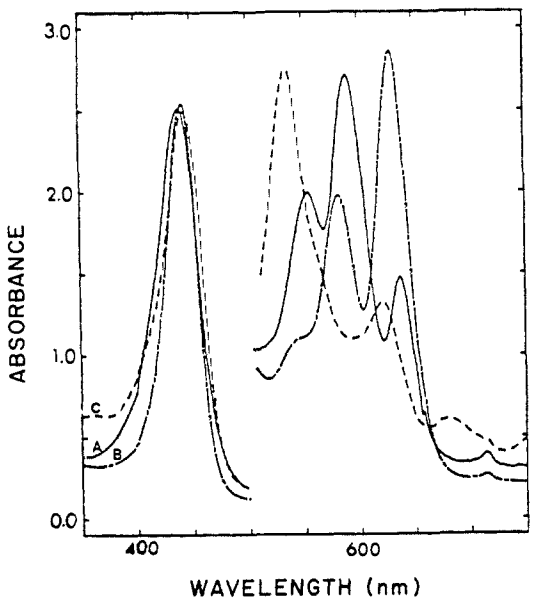

Figure 1. The electronic spectra of benzene solutions of (A) **2**, [TPP{C=C(p-C_6H_4Cl)$_2$H]Cl; (B) **1**, TPP{C=C(p-C_6H_4Cl)$_2$, formed by adding triethylamine to **2**; and (C) [TPP{C=C(p-C_6H_4Cl)$_2$H$_2$]$^{2+}$ formed by adding trifluoroacetic acid to **2**.

These reactions involve reaction of the N,N′-bridged porphyrin **1** or its monoprotonated, cationic form **2**. This bridged porphyrin

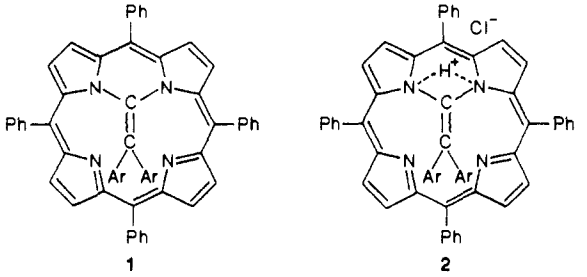

is available from the reaction of DDT (1,1,1-trichlorobis(p-chlorophenyl)ethane) with an iron(III) porphyrin halide in the presence of iron powder, followed by oxidation and demetalation.[7,8] Previous work has shown that the C–N bonds of the N,N′-bridge are susceptible to cleavage by low-valent metal complexes.[9] Treatment of **1** with nickel tetracarbonyl resulted in rupture of one C–N bond and addition of nickel to the center of the porphyrin as shown in Scheme I. With triiron dodecacarbonyl, both of the C–N bonds to the bridge are broken and the carbene complex, TPPFe{C=C(C_6H_4Cl)$_2$}, [10,11] is formed.

Results

Synthetic and Spectroscopic Studies. The N,N′-bridged porphyrin used in these studies exists in three forms. It is isolated by the procedure of Mansuy and co-workers[7] as the hydrated chloride salt **2**. This salt is readily deprotonated to give **1** by treatment with a suitable base, trimethylamine or 1,8-bis(dimethylamino)naphthalene. Figure 1 shows the electronic spectrum of **1**, obtained from **2** in the presence of triethylamine, and of **2**. The interconversion of **1** and **2** is reversible. Addition of trifluoroacetic acid to **1** restores the optical spectrum of **2**. Further addition of trifluoroacetic acid to **2** gives a diprotonated form whose electronic spectrum is shown in trace C of Figure 1. Either **1** or **2** can be used to form the ruthenium complexes described here, but the state of protonation does have some effect on the relative yield of different products.

Treatment of **2** with triruthenium dodecacarbonyl, under conditions usually used to incorporate ruthenium into porpyrins,[12,13] yields three products, **3**, **4**, and **5**. The latter two are quite similar. Both have suffered rupture of a corresponding pyrrole ring. In **5** the N,N′-bridging group is hydrogenated, whereas in **4** it is unsaturated as it is in the starting material. Procedures for giving optimal yields of each of these have been devised. The carbene

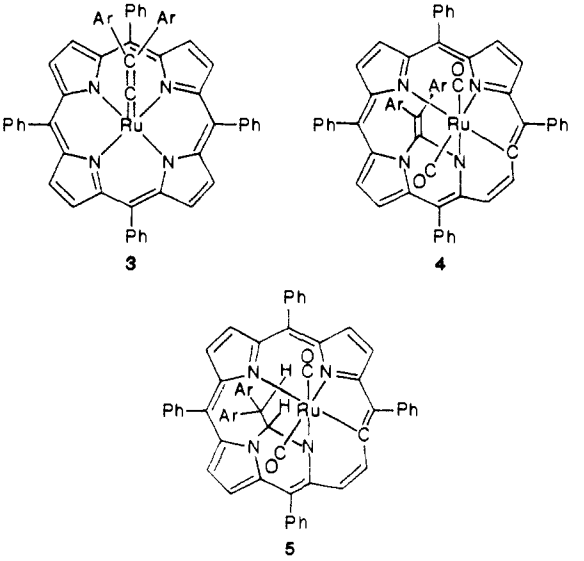

complex **3** is formed in 75% yield in the reaction of **2** with the carbonyl in boiling *N*,*N*-dimethylformamide solution. In tetrahydrofuran, the same reaction yields primarily **4** in 48% yield. The hydrogenated complex **5** is best obtained by the reaction of **1** with triruthenium dodecacarbonyl in tetrahydrofuran, but the yield is modest (30%), and 10% of **4** is obtained as well.

While routes which optimize the yield of either **4** or **5** have been devised, we have not discovered the species responsible for the olefin hydrogenation necessary to form **5**. Since the hydrides $H_2Ru_4(CO)_{13}$ and $H_4Ru_4(CO)_{12}$ are readily formed from triruthenium dodecacarbonyl,[14] we suspected that their presence might be responsible for the formation of **5**. However, reaction of **2** with either of these hydrides does not result in increased formation of **5**. In fact, **4** is formed in greater quantity than **5**. Similarly, attempts to convert **4** to **5** have not been successful. Exposure of boiling tetrahydrofuran solutions of **4** to dihydrogen, $H_2Ru_4(CO)_{13}$, or $H_4Ru_4(CO)_{12}$ did not produce **5**. Possibly trace amounts of ruthenium metal are responsible for the hydrogenation.

Spectroscopic data for these complexes are given in the experimental section and are in accord with the structural assignments. The infrared spectra of **4** and **5** show two terminal carbon monoxide stretching vibrations as expected for a cis pair of carbon monoxide ligands. The similarity in ν(CO) for these two compounds suggests that the ruthenium coordination in both is equivalent. No absorptions are seen in the infrared spectrum of **3** in the region 2500–1600 cm^{-1}: no carbon monoxide ligands are present. The electronic spectrum of **3** is that of a typical porphyrin with a strong Soret peak at 416 nm and weaker absorption at 522 nm. However, the spectra of **4** and **5** which are shown in Figure 2 are decidedly different and are indicative of disruption of the porphyrin. They lack a particularly strong feature that could be considered as a Soret peak, but they show instead a series of intense peaks in the ultraviolet and visible regions and weaker absorption at very low energies.

(7) Lange, M.; Mansuy, D. *Tetrahedron Lett.* **1981**, *22*, 2561.
(8) Wisnieff, T. J.; Gold, A.; Evans, S. A., Jr. *J. Am. Chem. Soc.* **1981**, *103*, 5616.
(9) Chan, Y. W.; Renner, M. W.; Balch, A. L. *Organometallics* **1983**, *2*, 1888.
(10) (a) Mansuy, D.; Lange, M.; Chottard, J. C. *J. Am. Chem. Soc.* **1978**, *100*, 3212. (b) **Note Added in Proof.** The X-ray crystal structure of the iron–carbene complex has recently been reported: Mansuy, D.; Battioni, J.-P.; Lavallee, D. K.; Fischer, J.; Weiss, R. *Inorg. Chem.* **1988**, *27*, 1052.
(11) Balch, A. L.; Chan, Y. W.; Olmstead, M. M.; Renner, M. W. *J. Org. Chem.* **1986**, *51*, 4651.
(12) Cullen, D.; Meyer, E., Jr.; Srivastava, T. S.; Tsutsui, M. *J. Chem. Soc., Chem. Commun.* **1972**, 584.
(13) Bonnett, J. J.; Eaton, S. S.; Eaton, G. R.; Holm, R. H.; Ibers, J. A. *J. Am. Chem. Soc.* **1973**, *95*, 2141.
(14) Bruice, M. I. In *Comprehensive Organometallic Chemistry*; Wilkinson, G., Stone, F. G. A., Able, E. W., Eds.; Pergamon: New York, 1982; Vol. 4, p 889.

Table I. Proton NMR Data from Chloroform-*d* Solutions at 25 °C

compound	chemical shifts (ppm), *J* (Hz)			
	pyrrole	phenyls	$(p\text{-}ClC_6H_4)_2C_2$	N-H
[TPPC=C(p-$C_6H_4Cl)_2$HCl] (**2**)	9.38 (d, *J* = 4.6, 2 H) 9.18 d, *J* = 5.0, 2 H) 9.09 (d, *J* = 4.4, 2 H) 8.55 (d, *J* = 4.0, 2 H)	8.38 (br, 4 H) 8.1–8.7 (m, 12 H) 7.14 (br, 4 H)	6.21 (d, *J* = 8.1, 4 H) 2.75 (br, 4 H)	−0.18 (s, 1 H)
TPPRu=C=C(p-$C_6H_4Cl)_2$ (**3**)	8.67 (s, 8 H)	8.10 (br, 4 H) 7.70 (br, 16 H)	6.43 (d, *J* = 8.0, 4 H) 3.98 (d, *J* = 8.0, 4 H)	
{TPPC=C(p-$C_6H_4Cl)_2$}Ru$(CO)_2$ (**4**)	9.41 (d, *J* = 10.3, 1 H) 8.14 (d, *J* = 10.3, 1 H) 7.65–7.4 (m, 4 H) 7.10 (d, *J* = 3.8, 1 H) 6.88 (d, *J* = 5.7, 1 H)	8.11 (d, *J* = 4.9, 1 H) 7.85 (d, *J* = 7.0, 2 H) 7.80 (d, *J* = 6.8, 2 H) 7.7–7.4 (m, 14 H) 6.70 (d, *J* = 7.2, 1 H)	7.03 (d, *J* = 7.7, 2 H) 6.02 (d, *J* = 8.1, 2 H) 5.66 (d, *J* = 7.7, 2 H) 4.88 (d, *J* = 8.1, 2 H)	
{TPPCHCH(p-$C_6H_4Cl)_2$}Ru$(CO)_2$ (**5**)	8.96 (d, *J* = 10.3, 1 H) 7.71 (d, *J* = 10.3, 1 H) 7.65–7.4 (m, 5 H) 6.71 (d, *J* = 5.3, 1 H)	8.16 (d, *J* = 7.1, 1 H) 7.75 (d, *J* = 7.0, 2 H) 7.65–7.4 (m, 16 H) 7.06 (d, *J* = 4.5, 1 H)	6.93 (d, *J* = 8.3, 2 H) 6.19 (d, *J* = 8.3, 2 H) 5.85 (d, *J* = 8.3, 2 H) 5.14 (d, *J* = 8.3, 2 H)	3.27 (d, *J* = 10.4, 1 H) 3.07 (d, *J* = 10.4, 1 H)

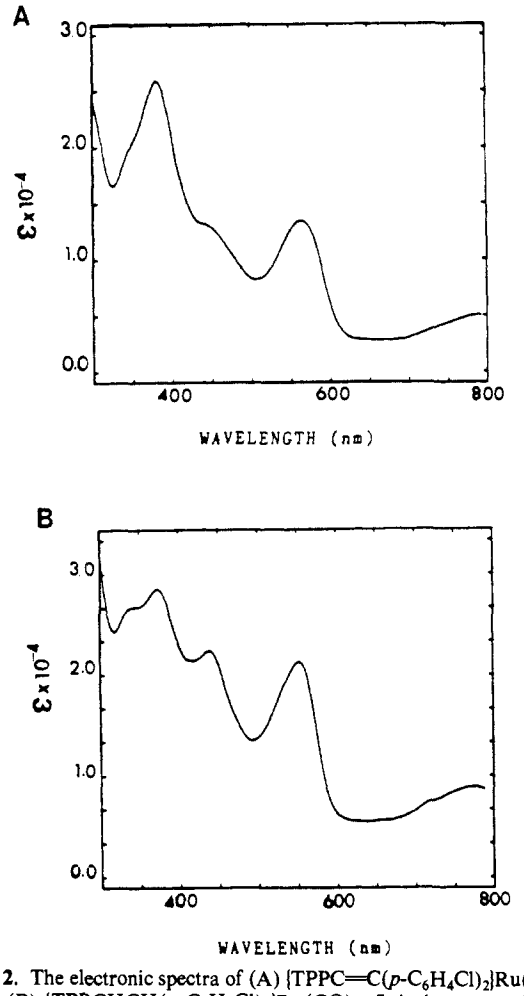

Figure 2. The electronic spectra of (A) {TPPC=C(p-$C_6H_4Cl)_2$}Ru$(CO)_2$, **4**, and (B) {TPPCHCH(p-$C_6H_4Cl)_2$}Ru$(CO)_2$, **5**, in benzene solution.

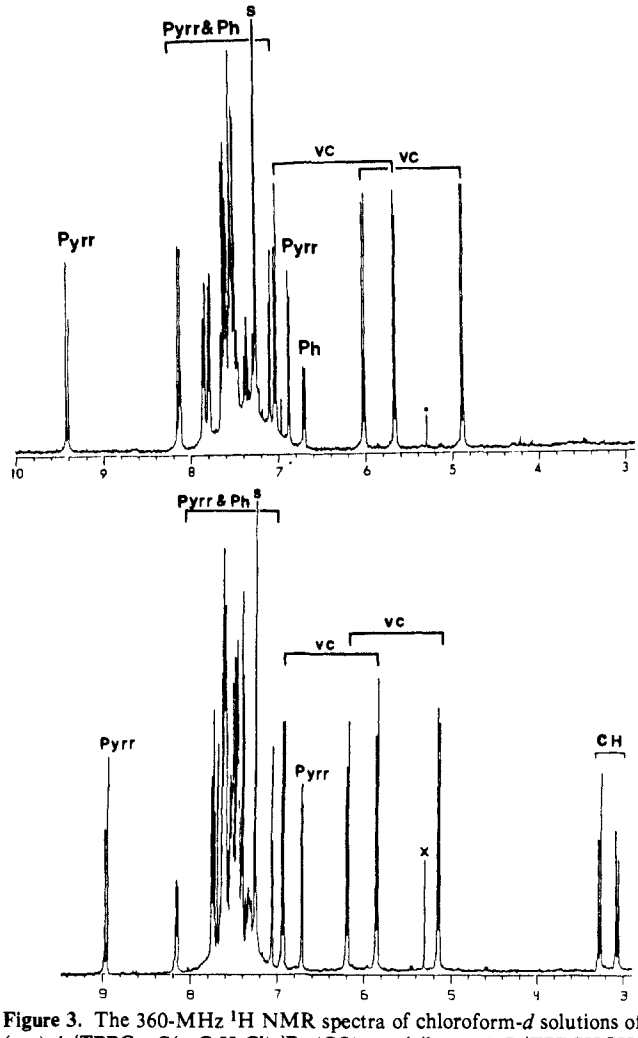

Figure 3. The 360-MHz ^{1}H NMR spectra of chloroform-*d* solutions of (top) **4**, {TPPC=C(p-$C_6H_4Cl)_2$}Ru$(CO)_2$, and (bottom) **5**, {TPPCHCH-(p-$C_6H_4Cl)_2$}Ru$(CO)_2$ at 25 °C. Pyrr, pyrrole protons; Ph, phenyl protons; VC, *p*-chlorophenyl protons; S, residual undeuteriated solvent; CH, protons of $CHCH(p\text{-}ClC_6H_4)_2$ group; X, impurities.

^{1}H NMR spectral data for the complexes are presented in Table I. The spectrum of **3** is relatively simple. A single pyrrole resonance at 8.67 ppm is consistent with the fourfold rotational symmetry expected for an unaltered porphyrin system. The *p*-chlorophenyl groups produce a characteristic quartet which shows a very significant upfield shift due to the ring current of the porphyrin. The overall pattern of this spectrum is quite similar to that of its iron analogue, TPPFe{C=C(p-$C_6H_4Cl)_2$}.[10,11] The spectra of **4** and **5**, which are shown in Figure 3, are much more complex since the symmetry of the porphyrin is destroyed. For each compound, eight resonances in the 7–5-ppm range have been assigned on the basis of intensity and coupling constants to the *p*-chlorophenyl protons. The pyrrole and phenyl resonances are found in the 6.5–9.0-ppm region, and several of the pyrrole resonances, which appear as well-separated doublets, have been identified as noted in Table I. For **5**, an AB quartet centered at 3.2 ppm is assigned to the aliphatic protons of the $CHCH(p\text{-}C_6H_4Cl)_2$ group.

The X-ray Crystal and Molecular Structure of {TPPCHCH-(p-$C_6H_4Cl)_2$}Ru$(CO)_2$ (5). In order to characterize **5** unambiguously, we undertook a crystallographic study. The structure of **4** was previously established.[6]

The atomic positional parameters for **5** are given in Table II (supplementary material). Tables III and IV give selected in-

Table III. Selected Interatomic Distances (Å)

ruthenium core	{TPPCHCH(p-ClC$_6$H$_4$)$_2$}-Ru(CO)$_2$ (5)	{TPPC=C(p-ClC$_6$H$_4$)$_2$}-Ru(CO)$_2$ (4)
Ru-N(1)	2.184 (8)	2.206 (5)
Ru-N(3)	2.260 (8)	2.257 (6)
Ru-N(4)	2.062 (8)	2.068 (5)
Ru-C(3)	2.126 (10)	2.086 (6)
Ru-C(2)	1.873 (11)	1.864 (6)
Ru-C(1)	1.882 (10)	1.878 (7)
C(23)-C(24)	1.520 (16)	1.343 (9)

Other Distances in {TPPCHCH(p-ClC$_6$H$_4$)$_2$}Ru(CO)$_2$

O(1)-C(1)	1.141 (13)	O(2)-C(2)	1.123 (13)
N(1)-C(6)	1.339 (13)	N(1)-C(23)	1.439 (12)
N(2)-C(8)	1.376 (13)	N(2)-C(11)	1.390 (12)
N(2)-C(23)	1.413 (11)	N(3)-C(13)	1.367 (12)
N(3)-C(16)	1.412 (13)	N(4)-C(18)	1.395 (12)
N(4)-C(21)	1.369 (11)	C(3)-C(4)	1.438 (15)
C(3)-C(22)	1.375 (14)	C(4)-C(5)	1.352 (15)
C(5)-C(6)	1.434 (14)	C(6)-C(7)	1.453 (14)
C(7)-C(8)	1.389 (13)	C(7)-C(71)	1.497 (15)
C(8)-C(9)	1.450 (14)	C(9)-C(10)	1.336 (14)
C(10)-C(11)	1.458 (14)	C(11)-C(12)	1.364 (14)
C(12)-C(13)	1.460 (14)	C(13)-C(14)	1.430 (15)
C(14)-C(15)	1.348 (15)	C(15)-C(16)	1.389 (13)
C(16)-C(17)	1.409 (14)	C(17)-C(18)	1.392 (13)
C(18)-C(19)	1.426 (13)	C(19)-C(20)	1.348 (14)
C(20)-C(21)	1.432 (14)	C(21)-C(22)	1.409 (14)

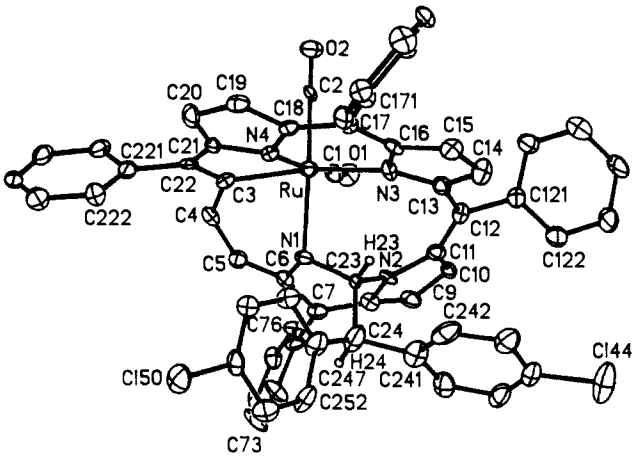

Figure 4. A perspective view of 5, {TPPCHCH(p-C$_6$H$_4$Cl)$_2$}Ru(CO)$_2$. Thermal ellipsoids are drawn at the 35% probability level. Hydrogen atoms are drawn as small circles.

teratomic distances and angles. For comparison, some selected data for 4 (from ref 6) are included. Figure 4 shows overall views of the structures of 4, while Figure 5 compares the structures of 4 and 5.

Both 4 and 5 have similar structures. In each, the pyrrole ring that once contained N(1)-C(6) has undergone rupture of the N(1)-C(3) bond. The perspective used in Figures 4 and 5 makes that clear. The nonbonded N(1)···C(3) distances in 4 and 5 are 2.732 and 2.741 Å, while normal pyrrole N-C distances are ~1.35 Å. As a result of the oxidative C-N bond rupture, the amide and carbanionic centers, N(1) and C(3), have become directly bonded to ruthenium by σ-bonds. The macrocycle is clearly no longer planar, although the large segment involving pyrrole rings containing N(3) and N(4) is itself rather flat, and the three intact pyrrole rings are planar. The nonplanarity of the macrocycle allows the two carbon monoxide ligands on ruthenium to occupy cis coordination sites.

The major difference between 4 and 5 involves the environment of C(23) and C(24). The C(23)-C(24) bond in 5 is a single bond with an appropriate bond distance (1.520 (16) Å), while in 4 it is a double bond and is shorter (1.343 (9) Å). In 4, the atoms N(2), C(23), N(1), C(24), C(242), C(247) are nearly planar, while in 5 this group is nonplanar and C(23) and C(24) assume tetrahedral geometry.

Table IV. Selected Interatomic Angles (deg)

ruthenium core	{TPPCHCH(p-ClC$_6$H$_4$)$_2$}-Ru(CO)$_2$ (5)	{TPPC=C(p-ClC$_6$H$_4$)$_2$}-Ru(CO)$_2$ (4)
N(1)-Ru-N(3)	93.7 (3)	93.0 (2)
N(1)-Ru-N(4)	101.1 (3)	100.4 (2)
N(3)-Ru-N(4)	85.7 (3)	86.1 (2)
N(1)-Ru-C(1)	85.4 (4)	86.4 (2)
N(3)-Ru-C(1)	100.8 (4)	102.8 (2)
N(4)-Ru-C(1)	170.6 (4)	168.5 (2)
N(1)-Ru-C(2)	171.8 (4)	173.6 (3)
N(3)-Ru-C(2)	91.9 (4)	89.1 (2)
N(4)-Ru-C(2)	85.4 (4)	85.7 (2)
C(1)-Ru-C(2)	87.6 (5)	87.2 (3)
N(1)-Ru-C(3)	78.6 (3)	79.3 (2)
N(3)-Ru-C(3)	158.5 (3)	158.8 (2)
N(4)-Ru-C(3)	76.3 (3)	76.0 (2)
C(1)-Ru-C(3)	98.6 (4)	96.5 (3)
C(2)-Ru-C(3)	98.1 (4)	100.6 (2)

Other Angles in 5

Ru-N(1)-C(23)	108.5 (5)	Ru-N(1)-C(6)	119.8 (7)
C(8)-N(2)-C(11)	110.4 (8)	C(6)-N(1)-C(23)	113.9 (8)
C(11)-N(2)-C(23)	133.7 (8)	C(8)-N(2)-C(23)	115.9 (7)
Ru-N(3)-C(16)	120.2 (6)	Ru-N(3)-C(13)	133.4 (7)
Ru-N(4)-C(18)	132.1 (6)	C(13)-N(3)-C(16)	106.3 (8)
C(18)-N(4)-C(21)	107.5 (7)	Ru-N(4)-C(21)	115.9 (6)
Ru-C(2)-O(2)	175.1 (10)	Ru-C(1)-O(1)	177.5 (9)
Ru-C(3)-C(22)	114.6 (7)	Ru-C(3)-C(4)	121.0 (7)
C(3)-C(4)-C(5)	124.3 (9)	C(4)-C(3)-C(22)	121.7 (9)
N(1)-C(6)-C(5)	121.1 (9)	C(4)-C(5)-C(6)	124.9 (10)
C(5)-C(6)-C(7)	116.6 (9)	N(1)-C(6)-C(7)	120.6 (9)
C(6)-C(7)-C(71)	122.2 (8)	C(6)-C(7)-C(8)	113.0 (9)
N(2)-C(8)-C(7)	117.5 (9)	C(8)-C(7)-C(71)	123.8 (9)
C(7)-C(8)-C(9)	134.1 (10)	N(2)-C(8)-C(9)	106.8 (8)
C(9)-C(10)-C(11)	109.9 (8)	C(8)-C(9)-C(10)	107.6 (9)
N(2)-C(11)-C(12)	125.5 (9)	N(2)-C(11)-C(10)	104.7 (8)
C(11)-C(12)-C(13)	128.5 (9)	C(10)-C(11)-C(12)	129.2 (9)
C(13)-C(12)-C(121)	113.6 (9)	C(11)-C(12)-C(121)	117.7 (9)
N(3)-C(13)-C(14)	109.5 (9)	N(3)-C(13)-C(12)	131.7 (9)
C(13)-C(14)-C(15)	106.2 (9)	C(12)-C(13)-C(14)	118.7 (9)
N(3)-C(16)-C(15)	107.8 (8)	C(14)-C(15)-C(16)	110.0 (9)
C(15)-C(16)-C(17)	123.3 (9)	N(13)-C(16)-C(17)	128.8 (8)
C(16)-C(17)-C(171)	117.6 (8)	C(16)-C(17)-C(18)	127.6 (9)
N(4)-C(18)-C(17)	121.0 (8)	C(18)-C(17)-C(171)	114.7 (8)
C(17)-C(18)-C(19)	131.5 (9)	N(4)-C(18)-C(19)	107.2 (8)
C(19)-C(20)-C(21)	106.7 (9)	C(18)-C(19)-C(20)	109.2 (9)
N(4)-C(21)-C(22)	115.9 (8)	N(4)-C(21)-C(20)	109.2 (8)
C(3)-C(22)-C(21)	114.8 (8)	C(20)-C(21)-C(22)	134.8 (9)
C(21)-C(22)-C(221)	117.7 (9)	C(3)-C(22)-C(221)	126.9 (9)
N(1)-C(23)-C(24)	117.4 (8)	N(1)-C(23)-N(2)	106.0 (8)
C(23)-C(24)-C(241)	106.5 (10)	N(2)-C(23)-C(24)	114.2 (8)
C(241)-C(24)-C(247)	113.1 (10)	C(23)-C(24)-C(247)	113.8 (9)

The ruthenium atoms in 4 and 5 have fairly regular, six-coordinate geometry that is characteristic of Ru(II) complexes. Most of the distortions from 90° and 180° bond angles can be ascribed to the constraints imposed by the macrocycle. Thus, the N(3)-Ru-C(3) angle (158.5 (3)°) is compressed significantly from linearity, and the N(1)-Ru-N(4) angle (101.1 (3)°) has opened up because of these constraints.

The C-C and C-N distances within the macrocycle's core show some degree of variation, but they are generally within ranges consistent with electron-delocalization within the π framework. Because of the strain imposed by the nonplanarity of the macrocycle, some bond lengthening is likely. Note, however, that the two isolated double bonds involving C(14)-C(15) (1.348 (15) Å) and C(19)-C(20) (1.348 (14) Å) are among the shortest of the C-C separations within the complex.

Inner Core Repair. The Conversion of 4 into 3. The damaged macrocycle in 4 is readily converted back to a normal porphyrin (eq 1). Heating a chlorobenzene solution of 4 at 130 °C produces the ^{1}H NMR spectral changes shown in Figure 6. New peaks, which are readily identified as belonging to the carbene complex 3, are observed to grow into the spectrum. As seen in trace C, the reaction is remarkably clean. Parallel experiments that monitor the electronic spectra show the growth of a Soret peak

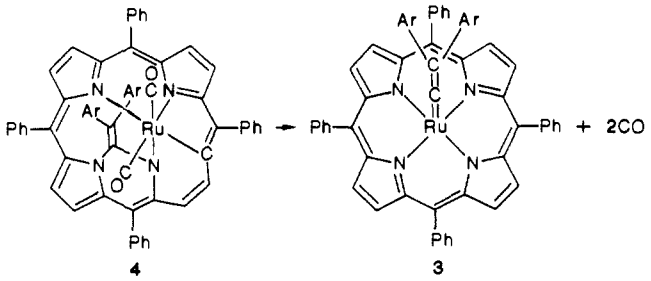

(1)

at 416 nm and a second band at 522 nm, while the absorbances of **4** decline in intensity. In a synthetic scale reaction, **4** has been converted into **3**, which has been isolated in 85% isolated yield from the chlorobenzene solvent.

Preliminary data suggest that **5** also undergoes a similar reaction in which the pyrrole (and porphyrin) ring reforms. On heating in toluene solution at 80 °C, the electronic spectrum of **5** changes and a new intense absorption at 438 nm, which we presume to be a Soret peak, grows.[15] Similarly in the ^{1}H NMR spectrum, the resonances of **5** decrease upon heating, while a new pyrrole resonance at 8.83 ppm and phenyl resonances at 8.18, 8.07, 8.05, and 7.49 ppm develop.[15] Unfortunately, in this case we have not been able to identify the axial ligand(s) on ruthenium.

Discussion

The reaction of triruthenium dodecacarbonyl with **1** and **2** is dominated by processes in which C–N bonds are broken. We view these as formal oxidative additions of the C–N bonds to ruthenium. The formation of **4** and **5** involves one such oxidative-addition and the formation of six-coordinate Ru(II) complexes from the Ru(0) starting material. The formation of **3**, which can be formally viewed as a Ru(IV) complex, involves two such oxidative-additions. The transformation of **4** into **3** can be viewed as proceeding by reductive elimination of N(1) and C(3) to reform the broken pyrrole ring,[16] followed by insertion of the resulting Ru(O) into the N(1)–C(23) and N(2)–C(23) bonds. Data to support these mechanistic hypotheses, however, are not available. The transformation of **4** to **3** clearly attests to the stability of the porphyrin ring.

These oxidative additions of C–N bonds to a metal, which are involved in the formation of **3**, **4**, and **5**, fall into a class of rarely observed reactions. In contrast, oxidative-additions of the slightly weaker P–C bonds to transition metals are more common.[17] One feature contributing to the low frequency of observation of oxidative-addition of C–N bonds to metal centers must be the infrequency with which amines are used as ligands in low-valent transition-metal complexes. The insertion of metal into C–N bonds may be important in the triruthenium dodecacarbonyl catalyzed scrambling of alkyl groups between tertiary amines.[18]

The electronic structure of the altered porphyrins in **4** and **5** can be considered as 18-π-heteroannulenes with two isolated double bonds as shown by resonance structures **6a** and **6b**. The

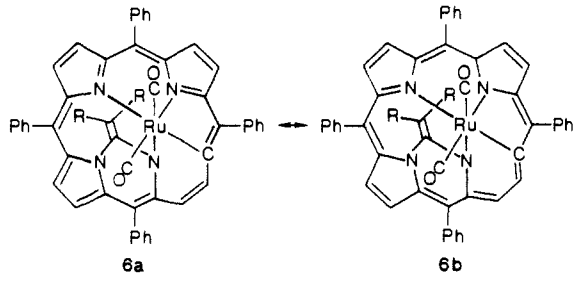

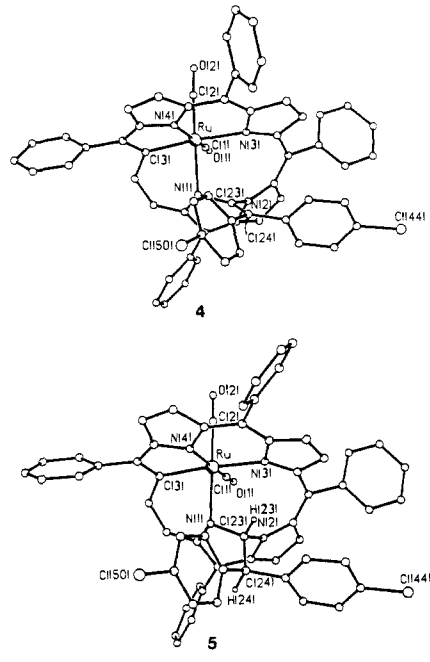

Figure 5. A comparison of the structures of **4** and **5** from similar perspectives.

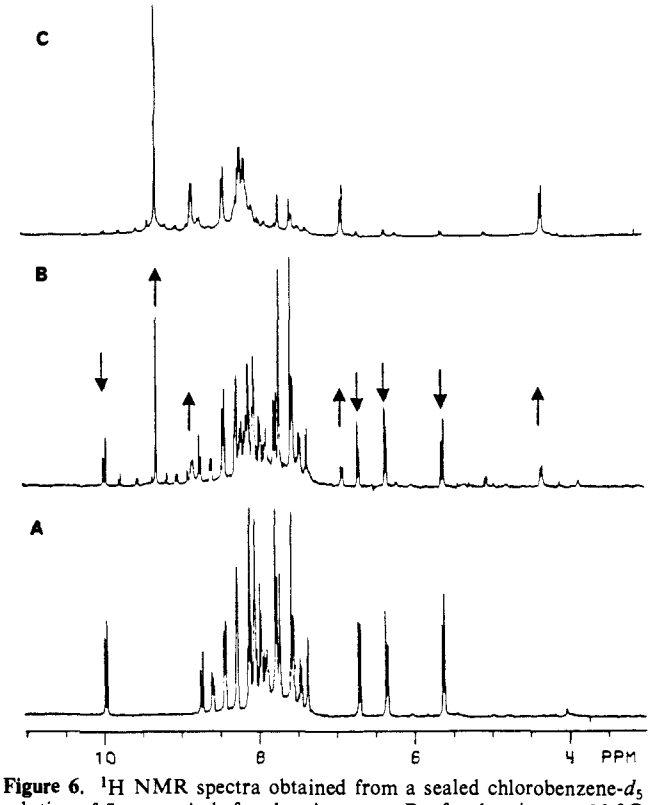

Figure 6. ^{1}H NMR spectra obtained from a sealed chlorobenzene-d_5 solution of **5**: trace A, before heating; trace B, after heating at 130 °C for 3 days; trace C, after heating at 130 °C for 10 days. Spectra were recorded at 25 °C.

severe nonplanarity of the macrocycles which is seen in the crystallographic work might be expected to interfere with conjugation within this system. However, the observation of the pyrrole resonances **4** and **5** in a downfield position and the *p*-chlorophenyl resonances in a position well upfield of the normal phenyl region follows the pattern seen in aromatic systems (for example, in **3**) and hence an aromatic ring current persists within the macrocycle in **4** and **5**. While the conjugated nature of the macrocycle is retained in **4** and **5**, the changes in the electronic structure are severe enough so that **4** and **5** no longer display electronic absorption spectra that are porphyrin-like.

(15) Figures showing these spectral changes can be found in the Ph.D. thesis of Y. W. Chan, University of California, Davis, 1985.
(16) A related example of C–N bond formation by reductive elimination from a porphyrin Fe(IV) phenyl complex has been reported: Balch, A. L.; Renner, M. W. *J. Am. Chem. Soc.* **1986**, *108*, 2603.
(17) Carty, A. *Pure Appl. Chem.* **1982**, *54*, 113.
(18) Shvo, Y.; Laine, R. M. *J. Chem. Soc., Chem. Commun.* **1980**, 753.

Table V. Crystal Data and Data Collection Parameters, Solution, and Refinement for {TPPCHCH(p-$C_6H_4Cl)_2$}Ru(CO)$_2$·$^1/_2CH_2Cl_2$ (5)

formula	$RuCl_3N_4O_2C_{60.5}H_{39}$
fw	1061.44
color and habit	dark red-purple plates
crystal system	monoclinic
space group	$P2_1/c$
a, Å	12.633 (7)
b, Å	19.293 (10)
c, Å	19.820 (9)
β, deg	95.59 (3)
V, Å^3	4808 (4)
T, K	130
Z	4
cryst dimens, mm	0.12 × 0.50 × 0.62
d_{calcd}, g cm^{-3} (130 K)	1.47
d_{measd}, g cm^{-3} (298 K)	1.41
radiation, Å	Mo Kα (λ = 0.71069)
μ(Mo Kα), cm^{-1}	5.4
range of transm. factors	0.79–0.95
diffractometer	$P2_1$, graphite monochromator
scan method	ω, 1.5° range, 1.2° offset for bkgnd
scan speed, deg min^{-1}	60
2θ range, deg	0–45
octants collected	h, k, $\pm l$
no. of data collected	6850
no. of unique data	6291, R(merge) = 0.08
no. of data used in refnmt	4172 [$1 > 2\sigma(1)$]
no. of parameters refined	640
R^a	0.079
$R_w{}^a$	0.081 [$w = 1/(\sigma^2(F_o))$]

$^a R = \sum||F_o| - |F_c||/F_o|$ and $R_w = \sum||F_o| - |F_c||w^{1/2}/\sum|F_o w^{1/2}|$.

Experimental Section

Preparation of Compounds. Triruthenium dodecacarbonyl and 1,8-bis(dimethylamino)naphthalene were obtained from Aldrich Chemical Company. [TPPC=C(p-$C_6H_4Cl)_2$H]Cl (**2**) was obtained as described previously.[7,8] Tetrahydrofuran was dried and distilled from sodium/benzophenone under nitrogen before use. *N,N*-Dimethylformamide was dried over 4A molecular sieves. Chlorobenzene was passed through a column of basic alumina immediately before use. Dichloromethane was distilled from phosphorus pentoxide under nitrogen.

TPPRu=C=C(p-$C_6H_4Cl)_2$ (3). *N,N*-Dimethylformamide (25 mL) was placed in a 50-mL, two-neck flask equipped with a reflux condensor and a sidearm containing 41 mg (0.064 mmol) of triruthenium dodecacarbonyl and 48 mg (0.056 mmol) of **2**. The *N,N*-dimethylformamide was boiled under reflux for 5 min under an argon atmosphere. The solid reagents were added to the boiling solution which was maintaining under reflux for 30 min. After being cooled, the solvent was removed under vacuum. The solid residue was dissolved in benzene and applied to a dry silica gel column (2 in. × 8 in.). Elution with hexane gave a yellow band which contained triruthenium docecacarbonyl. Elution with 2/1 (v/v) benzene/hexane removed a red band while final elution with dichloromethane gives an orange band. This was collected and evaporated to dryness. Recrystallization of this material by dissolution in dichloromethane, filtration, and the gradual addition of acetonitrile gave the product as purple microcrystals (yield 40 mg, 75%). Anal. Calcd for $C_{58}H_{36}Cl_2N_4Ru$: C, 72.50; H, 3.78; N, 5.83; Cl, 7.38. Found: C, 72.73; H, 4.09; N, 6.72; Cl, 7.20. UV/vis λ_{max} nm (ϵ, mM^{-1} cm^{-1}) 416 (71.9), 522 (15.2).

{TPPC=C(p-$C_6H_4Cl)_2$}Ru(CO)$_2$ (4). An oxygen-free solution of 32 mg (0.050 mmol) of triruthenium dodecacarbonyl and 43 mg (0.050 mmol) of TPP{C=C(p-$C_6H_4Cl)_2$}HCl (**2**) in 30 mL of tetrahydrofuran was boiled under reflux in a static argon atmosphere for 3 h. The solution turned from green to red during this process. The solvent was removed under vacuum. The solid residue was dissolved in benzene and applied to a dry silica gel column (2 in. × 8 in.). Elution with hexane removed a yellow band containing triruthenium docecacarbonyl. Elution with 2/1 (v/v) benzene/hexane gave a red solution. This was concentrated and subject to centrifugal chromatography with use of a 1 mm thick silica gel disc. The sample was eluted with 5% benzene in pentane which gave a purple band of the desired product **4** followed by a red-purple band which contained {TPPCHCH(p-$C_6H_4Cl)_2$}Ru(CO)$_2$ (**5**). Each band was collected and evaporated to dryness. Recrystallization of the residue from the purple band by dissolution in dichloromethane, filtration, and gradual addition of acetonitrile gave 29 mg (48%) of **4** as purple crystals. Recrystallization of the residue from the red-purple band by the same method gave 5 mg (8%) of **5**. Spectroscopic data for **4**: UV/vis, 382 (25.9), 442 (sh), 564 (13.4), 784 (4.5); IR ν(CO) 2026, 1945 cm^{-1}; field desorption mass spectrum, most intense peak in parent ion cluster, 1016 amv.

{TPPCHCH(p-$C_6H_4Cl)_2$}Ru(CO)$_2$ (5). This was best obtained by using the procedure described above for **4** with the addition of 5 equiv of 1,8-bis(dimethylamino)naphthalene (a noncoordinating base) to initial reaction. After separation and recrystallization as described above, a 30% yield of the desired product **5** was obtained. In addition, a 10% yield of **4** was obtained. No **3** was obtained from this reaction. Spectroscopic data for **5**: UV/vis, 374 (29.2), 438 (23.6), 552 (21.3), 772 (7.4); IR ν(CO) 2020, 1938 cm^{-1}.

Conversion of {TPPC=C(p-$C_6H_4Cl)_2$}Ru(CO)$_2$ (4) into TPPRu=C=C(p-$C_6H_4Cl)_2$ (3). A solution of 20 mg of **4** in 50 mL of oxygen-free chlorobenzene was boiled under reflux in an argon atmosphere for 24 h. After being cooled, the solvent was removed under reduced pressure. Chromatography of the residue on silica gel with dichloromethane as the eluant gave an orange band. This was collected and recrystallized from dichloromethane/acetonitrile to give 16 mg (85%) of **3** as purple crystals. These were identified by UV/vis, infrared, and ^{1}H spectroscopy.

Physical Measurements. Electronic spectra were recorded on a Hewlett-Packard 8450A spectrophotometer. Infrared spectra were recorded on a Perkin-Elmer 180 spectrometer. ^{1}H NMR spectra were obtained on a Nicolet NT360 FT NMR spectrometer operating in the quadrature mode. Field desorption mass spectra were obtained from the mass spectroscopy resource at the University of California, San Francisco.

X-ray Structure Determination and Refinement of {TPPCHCH(p-$C_6H_4Cl)_2$}Ru(CO)$_2$·$^1/_2CH_2Cl_2$, (5). Suitable crystals were obtained by the slow diffusion of acetonitrile into a dichloromethane solution of **5** at −10 °C over a 3-week period. A crystal was mounted on a glass fiber with silicone grease and positioned in the cold stream of the diffractometer with the longest dimension of the crystal parallel to ϕ. Crystal data and data collection parameters are given in Table V. No decay in the intensities of two standard reflections was observed during the course of data collection.

The usual corrections for Lorentz and polarization effects were applied to the data. Crystallographic programs used were those of SHELXTL, version 4, installed on a Data General Eclipse computer. Scattering factors and corrections for anomalous dispersion were from the *International Tables*.[19]

Solution of the structure was accomplished by Patterson methods. Hydrogen atoms were included by use of a riding model, with a C–H length of 0.96 Å and isotropic thermal parameters for the hydrogen atoms equal to 1.2 times that of the bonded carbon. An absorption correction was applied.[20] One low-angle reflection that was affected by extinction was removed from the data. The half-molecule of dichloromethane is located near the center of symmetry, which generates a second chlorine, as well as a second associated carbon atom. This carbon atom is therefore disordered and was assigned an occupancy of 0.5. In the last cycles of refinement, all non-hydrogen atoms were assigned anisotropic thermal parameters. In the final difference map the largest feature was 2.2 e Å^{-3} in height, 1.04 Å from Ru. The remaining peaks were all less than 0.65 e Å^{-3}. The somewhat large R factors are a reflection of the marginal crystal quality and the rapid data collection method. They do not reflect disagreement with the model.

Acknowledgment. This work was supported by the National Institutes of Health (GM26226).

Registry No. 1, 87532-88-5; **2**, 79311-04-9; **3**, 87532-89-6; **4**, 90194-59-5; **5**, 114299-72-8; $Ru_2(CO)_{12}$, 15243-33-1.

Supplementary Material Available: Listings of atomic coordinates, all bond lengths and angles, anisotropic thermal parameters, and hydrogen atom positions for **5** (9 pages); tables of structure factors for **5** (25 pages). Ordering information is given on any current masthead page.

(19) *International Tables for X-ray Crystallography*; Kynoch: Birmingham, England, 1974; Vol. IV.

(20) The absorption correction program XABS obtains an adsorption tensor from $F_o - F_c$ differences. Hope, H.; Moezzi, B. Department of Chemistry, University of California, Davis.